Nanotechnology, Science and Applications

Dovepress
Taylor & Francis Group

Open Access Full Text Article

ORIGINAL RESEARCH

Multimodal Nanobiophysical Profiling of Melanoma-Derived Small Extracellular Vesicles Reveals Glycan Signatures Associated with Tumor Progression

Swamy Kasarla[1], Karolina Staniak[1,2], Magdalena Surman[3], Krystian Zajączkowski[1], Alicja Targońska[2], Grażyna Mosieniak[2], Konstancja Bobecka-Wesołowska[4], Josef Uskoba[5], Małgorzata Przybyło[3], Tomasz Kobiela[1]

[1]Laboratory of Biomolecular Interactions Studies, Chair of Drug and Cosmetics Biotechnology, Faculty of Chemistry, Warsaw University of Technology, Warsaw, Poland; [2]Laboratory of Cytometry, Nencki Institute of Experimental Biology, Polish Academy of Sciences, Warsaw, Poland; [3]Department of Glycoconjugate Biochemistry, Institute of Zoology and Biomedical Research, Faculty of Biology, Jagiellonian University in Krakow, Krakow, Poland; [4]Faculty of Mathematics and Information Science, Warsaw University of Technology, Warsaw, Poland; [5]BioTech A.s., Prague, Czech Republic

Correspondence: Tomasz Kobiela, Laboratory of Biomolecular Interactions Studies, Chair of Drug and Cosmetics Biotechnology, Faculty of Chemistry, Warsaw University of Technology, 3 Noakowskiego Street, Warsaw, 00-664, Poland, Email tomasz.kobiela@pw.edu.pl

Purpose: Small extracellular vesicles (sEVs) are nanoscale biomaterial-like structures involved in intercellular communication and cancer progression. Aberrant surface glycosylation may serve as a diagnostic marker for malignancy. This study aimed to compare the size, glycosylation, and biophysical properties of sEVs secreted by primary and metastatic melanoma cells, and to evaluate a novel analytical technique for glycoprofiling.

Methods: sEVs were isolated from the primary (WM115) and metastatic (WM266-4) melanoma cell lines. Their size and concentration were assessed via Nanoparticle Tracking Analysis (NTA), and exosomal identity was confirmed using Western blotting. Glycosylation profiling was performed using a multimodal strategy: Quartz Crystal Microbalance with Dissipation monitoring (QCM-D), Nanoplasmonic Sensing (NPS), and, for the first time, Flow-Induced Dispersion Analysis (FIDA). Concanavalin A (Con A) was used as the probe for high-mannose glycans.

Results: WM266-4-derived sEVs were significantly larger, whereas WM115 cells secreted more vesicles. Western blotting confirmed the presence of exosomal markers and absence of organelle contaminants. QCM-D and NPS showed stronger Con A binding and higher glycan viscoelasticity index (gVI) in metastatic sEVs, indicating altered glycan architecture. FIDA further confirmed these differences by quantifying a lower dissociation constant (Kd) and multivalent binding behavior in WM266-4-derived sEVs, consistent with a denser glycan coat.

Conclusion: Metastatic melanoma–derived sEVs exhibited distinct Con A–detectable high-mannose glycosylation patterns that may represent malignancy-associated features. This study demonstrates the utility of multimodal nanobiophysical methods, particularly FIDA, as sensitive tools for EV glycoprofiling. While the present findings are based on cell line–derived sEVs, they support the translational potential of glycan-based signatures for future liquid biopsy platforms and expand the analytical capabilities of cancer nanodiagnostics.

Plain Language Summary: Melanoma is a dangerous type of skin cancer that can spread quickly. Doctors need better ways to tell how aggressive a melanoma is, ideally using simple blood tests. One promising source of information is small extracellular vesicles (sEVs). These nanosized particles are released by all cells, including cancer cells, and carry biological signals that may reveal disease status. In this study, researchers compared sEVs released by two melanoma cell lines: one from an early-stage tumor (WM115) and one from a later, metastatic tumor (WM266-4). Both came from the same patient, making the comparison more reliable. The team found that metastatic cells produced fewer but larger vesicles, with clear differences in the sugar molecules (glycans) displayed on their surfaces. To study these sugar patterns, the researchers combined advanced nanoscale tools: Quartz Crystal Microbalance with

Received: 18 June 2025
Accepted: 29 October 2025
Published: 6 November 2025

Dissipation (QCM-D), NanoPlasmonic Sensing (NPS), and, for the first time in this context, Flow-Induced Dispersion Analysis (FIDA). Using a plant protein called Concanavalin A (Con A), which specifically binds to high-mannose glycans, they showed that vesicles from metastatic cells carried denser and more accessible sugar motifs. These findings suggest that vesicle surface sugars could provide useful clues about melanoma progression. However, the results come from cell line–derived vesicles and have not yet been validated in patient samples. Future studies using broader lectin panels and clinical material will be needed. Even so, this research highlights the potential of glycan signatures and FIDA as part of future non-invasive, nanotechnology-enabled blood tests to monitor cancer.

Keywords: small extracellular vesicle, sEVs, glycosylation profiling, melanoma progression, lectin–glycan interactions, biophysical characterization, metastatic cancer, metastasis-associated marker

Graphical Abstract

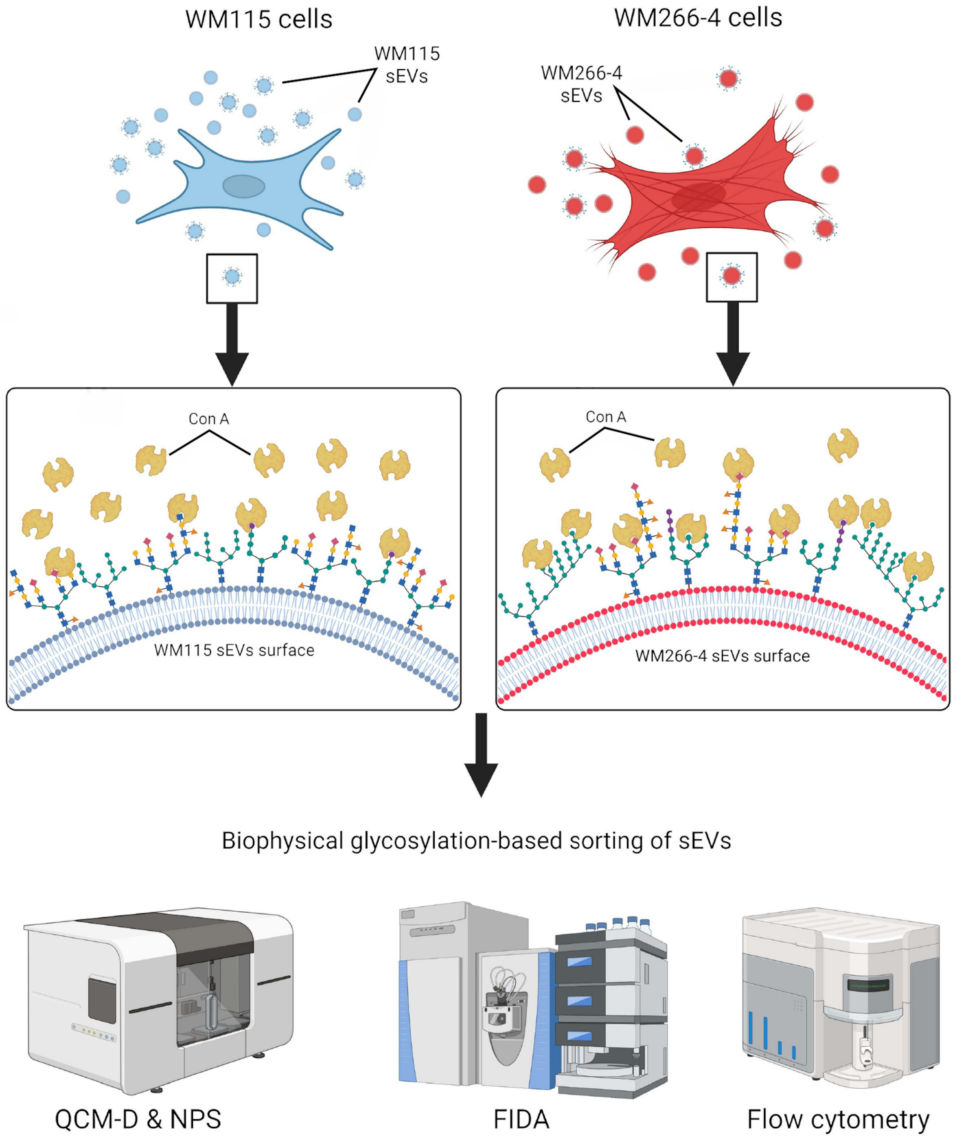

Introduction

Cutaneous melanoma is widely recognized as the most aggressive type of skin cancer worldwide. According to the GLOBOCAN 2022 database, melanoma accounts for approximately 3.2% of all new cancer cases globally, with an estimated 331,722 new cases reported by 2022. Despite its lower incidence compared to other skin cancers, melanoma is responsible for a disproportionately high number of skin cancer-related deaths owing to its rapid proliferation, early metastatic potential, and the limited effectiveness of current therapies in the metastatic stage. Unlike most malignancies, the incidence of cutaneous melanoma continues to rise globally every year, further emphasizing the pressing need for effective early detection and prognostic strategies.[1]

Recent therapeutic advances, particularly immune checkpoint inhibitors and targeted therapies, have resulted in measurable declines in melanoma mortality in many high-income countries, including US,[2] Sweden,[3] and Iceland.[4] However, melanoma continues to represent a significant health burden worldwide, underscoring the importance of improved early detection strategies.[5] Consequently, early diagnosis remains the cornerstone for clinical success. According to Breslow's thickness classification, of 95–100%, those exceeding 4 mm show significantly poorer outcomes, with survival dropping to 37–50%.[6] This stark contrast underscores the need for sensitive and specific diagnostic tools that can detect melanoma in its early stages.

Melanoma progression from a localized lesion to systemic metastasis involves complex genetic and epigenetic reprogramming, including the epithelial-mesenchymal transition (EMT). EMT confers invasive properties, enabling melanoma cells to detach, invade surrounding tissues, enter the circulation, and eventually form distant metastases.[7] This transition is also accompanied by changes in cell surface molecules such as glycosylated adhesion proteins, which facilitate tissue invasion and immune evasion.[8] Recent studies have shown that melanoma cells undergoing EMT-like phenotype switching also release extracellular vesicles (EVs) with altered molecular cargo, which reflects this phenotypic shift and can be tracked as indicators of drug resistance and metastatic progression.[9–13] In this context, understanding the molecular underpinnings of EMT and the mechanisms supporting metastatic spread is essential for identifying effective diagnostic and therapeutic targets.

A growing body of evidence points to the pivotal role of EVs, particularly small extracellular vesicles (sEVs, often referred to as exosomes), in melanoma progression and metastasis. These nano-sized vesicles, secreted by tumor and stromal cells under both physiological and pathological conditions, mediate intercellular communication and actively modulate the tumor microenvironment. Small EVs released by melanoma cells carry molecular cargo that enhances invasion, migration, immune evasion, and pre-metastatic niche formation. Notably, both the quantity and molecular composition of sEVs, particularly their glycoprotein content, differ markedly between healthy and malignant conditions, positioning them as promising, minimally invasive biomarkers for disease detection and monitoring.[14–18]

Glycosylation is a dynamic post-translational modification regulated by cellular signaling and metabolic state. Importantly, recent research has emphasized the diagnostic significance of glycosylation patterns in EVs, including sEVs, across a range of pathological states. Li et al demonstrated that glycosylation influences EV biogenesis, cellular uptake, and disease-specific interactions. Their comprehensive review highlighted how EV glycans, especially N-glycans and sialylated structures, can serve as key biomarkers and therapeutic targets, reinforcing the growing relevance of glycosylation-focused approaches in cancer biomarker discovery and clinical diagnostics.[19]

Although most current diagnostic efforts rely on the detection of static protein markers, they often fail to capture the full complexity and dynamic nature of disease progression. Unlike protein epitopes, which remain structurally conserved over time, glycosylation is a highly dynamic and post-translationally regulated process that reflects changes in cellular physiology, oncogenic signaling, and therapy-induced stress. This makes glycans highly responsive and temporally relevant indicators of the disease state an advantage increasingly recognized in biomarker research.

One crucial aspect of melanoma biology is altered glycosylation of the cell surface and secreted proteins. Aberrant glycan patterns are closely associated with malignant cell behavior and influence adhesion, motility, proliferation, and immune interactions. In our previous study, we proposed a diagnostic model based on lectin–glycan binding analysis in combination with biophysical detection platforms, revealing the diagnostic potential of glycan signatures.[20,21] Building on this foundation, the present study investigated whether the glycosylation profiles of sEVs secreted by melanoma cells

reflect changes in their cells of origin and whether these profiles differ between the primary and metastatic stages of melanoma progression.

While previous studies have established the diagnostic relevance of EV glycosylation in other cancers and explored biophysical tools for EV characterization, they largely focused either on global vesicle heterogeneity or on single analytical modalities. For example, Williams et al provided one of the first systematic reviews of EV glycosylation, emphasizing its biomarker potential but without experimentally linking glycan dynamics to defined stages of tumor progression.[22] More recently, Li et al reviewed advances in EV glycomics and highlighted N-glycans and sialylated structures as key diagnostic targets, reinforcing the clinical relevance of glycosylation-centered approaches. Another review on EV glycosylation was published by Vroblova et al, with particular focus on lectins as tools for EV isolation, EV glycan profiling, and for cancer detection and monitoring based on their binding to tumor-derived EVs.[23]

Furthermore, in breast cancer, Saroj et al probed aberrantly glycosylated MUC1 on EVs using biochemical assays combined with Fourier-Transformed Infra-Red Spectroscopy (FT-IR) and multivariate analysis, demonstrating that glycan features can be discriminated in a label-free fashion.[24] Complementing these, Zhang et al applied a lectin-induced aggregation strategy with Dynamic Light Scattering (DLS) readout to translate glycan expression into size-based signals for cancer diagnostics.[25] Lectin-based microarray was also applied by Sun et al to profile exosomes from colorectal cancer (CRC) cell lines and CRC tumor-bearing mice. The study demonstrated that out of 27 different lectins, Ulex Europaeus Agglutinin I (UEA I) (recognizing α1,2-linked L-fucose) bears potential to discriminate different CRC subtypes and to track disease progression.[26]

Our study advances the field by implementing a multi-platform nanobiophysical strategy integrating Nanoparticle Tracking Analysis (NTA), Quartz Crystal Microbalance with Dissipation (QCM-D) combined with Nanoplasmonic Sensing (NPS), and Flow-Induced Dispersion Analysis (FIDA), with validation by flow cytometry to resolve glycan–lectin interaction profiles (focusing on mannose residues probed by Concanavalin A, Con A) on melanoma-derived sEVs that reflect the progression from primary to metastatic disease. In contrast to static analyses of single glycoproteins or ensemble size-based readouts, this approach captures dynamic and functional glycan signatures linked to melanoma phenotype switching and therapy resistance. By integrating complementary label-free methods sensitive to particle heterogeneity, viscoelastic properties, refractive index, and molecular binding parameters, our work moves beyond descriptive glycomic profiling toward a quantitative, mechanistically grounded framework for sEV-based melanoma diagnostics. Recent advances in label-free biophysical detection platforms have strengthened the relevance of this approach. Mazouzi et al applied QCM-D combined with NPS to distinguish EV subpopulations in a Huntington's disease model, detect changes in viscoelastic properties linked to pathological transformation, and demonstrate the diagnostic potential of physical EV traits across diverse diseases.[27]

Materials and Methods

Cell Lines and Culture Conditions

The melanoma cell lines used in this study, namely WM115 (primary vertical growth phase) and WM266-4 (the lymph node metastasis) - isogenic pair (primary/metastatic) of cutaneous melanoma cell lines were obtained from the ESTDAB Melanoma Cell Bank (Tübingen, Germany). The cells were cultured in RPMI-1640 medium containing L-glutamine (VWR, Radnor, PA, USA) supplemented with 10% fetal bovine serum (Life Technologies, Carlsbad, CA, USA) and an antibiotic-antimycotic solution (Sigma-Aldrich, St. Louis, MO, USA, A5955). All cells were cultured under standard conditions (5% CO_2 and 37°C), passaged after reaching approximately 85% confluence, and collected by trypsinization using a 0.05% trypsin–EDTA solution (Life Technologies, Carlsbad, CA, USA).

Isolation of Small Extracellular Vesicles (sEVs)

sEVs released by primary (WM115) and metastatic (WM266-4) cells were isolated from conditioned media by sequential centrifugation, according to a previously protocol described in.[28] Cells were cultured in medium supplemented with EV-free serum until reaching ~85% confluence to obtain conditioned medium (CM). EVs-free serum was obtained from fetal bovine serum (Life Technologies, Carlsbad, CA, USA) ultracentrifugation at 140,000 × g and 4°C for 18 h. Then, CM

was collected and centrifuged using MPW-350R centrifuge at 1280 × g and 4°C for 20 min. The supernatant was collected and centrifuged in a Beckman Coulter Optima XPN-100 Ultracentrifuge at 16,500 × g and 4°C for 20 min in a Type 70 Ti rotor. After that, the supernatant was transferred to fresh polycarbonate centrifuge bottles and centrifuged at 118,000 × g at 4°C for 70 min using a Type 70 Ti rotor. The obtained sEV pellet was suspended in 100 µL of fresh Phosphate Buffered Saline (PBS) and stored at − 80°C for further analysis (Figure 1). For the WM266-4 and WM115 cells, sEVs were isolated from at least 11 independent biological experiments.

Assessment of Quality and Purity of Isolated sEVs Samples

Size Measurement and Concentration Determination

The size and concentration of the isolated sEVs were determined using NanoSight NS300 (Malvern Instruments Ltd., UK). Samples were prepared for measurement by dilution in PBS (1:500). For each sample, data acquisition was performed using the NanoSight NS300 system, with five 30-second video recordings captured and analyzed in real time using the built-in NanoSight NTA Software 3.4.4; these videos were not intended for use as supplementary material. All experiments were performed with 11 biological replicates for both cell lines; the number of biological replicates (n) is shown in Figure 2. To compare two samples (mean diameter of sEVs released by WM115 and WM266-4 melanoma cells and the number of sEVs released by 1000 WM115 cells and 1000 WM266-4 cells), *t*-test (in case of normality and equality of variances) or non-parametric Mann–Whitney test (when the requirements of *t*-test were not met) were used. Statistical analyses were performed using Prism 10.2.3 (GraphPad Software Inc., La Jolla, CA, USA).

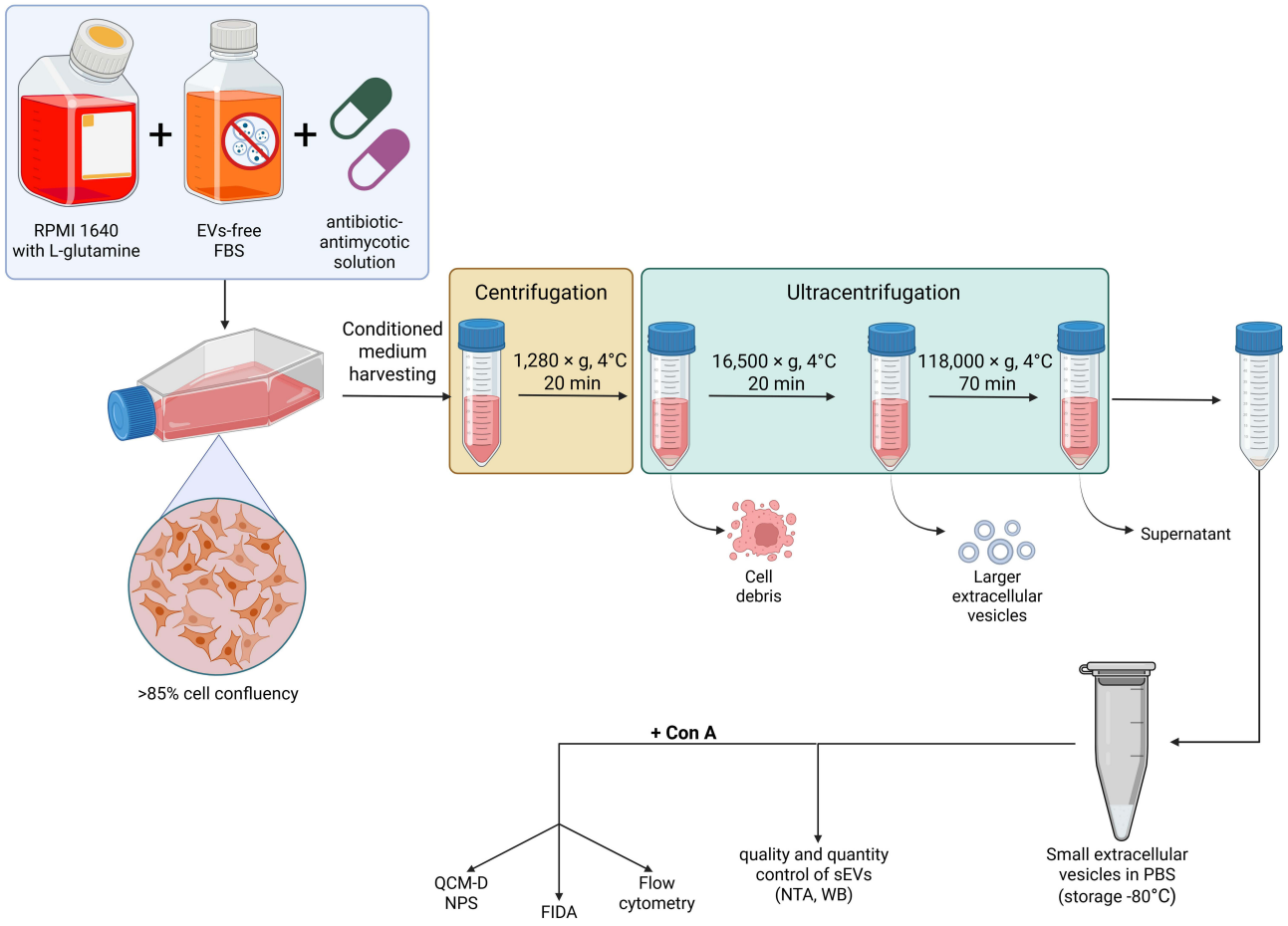

Figure 1 Workflow illustrating the stepwise procedure for the isolation of exosomes from WM115 and WM266-4 melanoma cell supernatants and their subsequent characterization and application in downstream experiments.

https://doi.org/10.2147/NSA.S547649

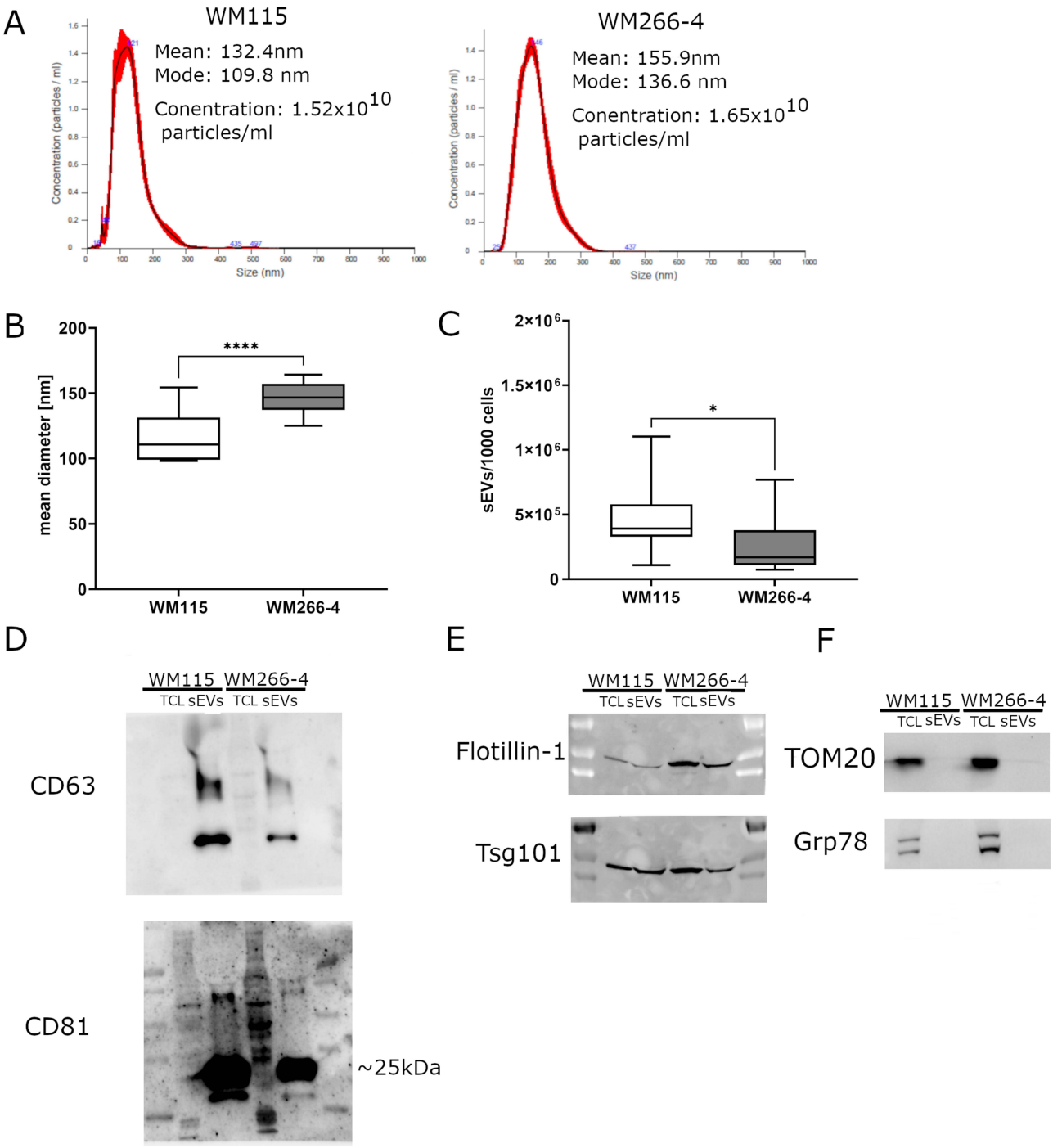

Figure 2 Characterization of sEVs isolated from primary (WM115) and metastatic (WM266-4) melanoma cells. (**A**) The representative plot of the size and concentration measurements of sEVs released by WM115 and WM266-4 melanoma cells using NTA. (**B**) Quantitative analysis of the size of sEVs released by WM115 and WM266-4 melanoma cells measured by NTA. n=11; Statistical significance of difference between mean diameter of sEVs released by WM115 and WM266-4 melanoma cells was confirmed by results of the *t*-test (**** $p \leq 0.0001$). (**C**) The total number of sEVs released by WM115 and WM266-4 melanoma cells measured by NTA. n=11; Boxes: Q1, median, Q3; error bars: minimum, maximum. Statistical significance of difference between number of sEVs released by 1000 WM115 cells and 1000 WM266-4 cells was confirmed by results of the Mann–Whitney test (* $p \leq 0.05$). (**D**–**F**). Western blotting analysis of exosome surface markers (CD81, CD63 – panel **D**), exosome membrane and cargo markers (Flotillin-1 and Tsg101 – panel **E**), Golgi (Grp78 – panel (**F**) and mitochondrial markers (TOM20 – panel (**F**) in isolated sEV fraction (sEVs) and total cell lysate (TCL) from WM115 and WM266-4 melanoma cells (20 µg of each sample).

Western Blotting Analysis

sEVs were lysed in reducing (with 100 mM dithiothreitol) or non-reducing (without dithiothreitol) sample buffer (62.5 mM Tris–HCl pH 6.8 containing 2% SDS, 10% glycerol and 0.2% bromophenol blue). Then Samples were denatured for

10 min at 95°C. Equal amounts of protein (20 μg) were separated on 15% sodium dodecyl sulfate-polyacrylamide gels and transferred onto nitrocellulose membranes. Membranes were blocked with 5% non-fat dry milk or 5% bovine serum albumin (BSA) dissolved in TBS (20 mM Tris-HCl, pH 7.6; 0.137 M NaCl) containing 0.1% Tween 20 for 1 h at RT and incubated overnight at 4°C with mouse anti-CD81, anti-CD63, rabbit anti-Tsg101, anti-Grp78 (Abcam, Cambridge, United Kingdom; dilution 1:250–1:500); mouse anti-Flotillin-1 (BD Biosciences, Franklin Lakes, NJ, USA; dilution 1:500), rabbit anti-TOM20 (Proteintech, Rosemont, Il, USA; dilution 1:1000) dissolved in TBS containing 0.1% Tween 20 and 5% milk/BSA. Following incubation with the appropriate horseradish peroxidase-conjugated secondary antibody (Vector Laboratories, Newark, CA, USA; dilution 1:2000) for 1 h at RT, proteins were detected using an ECL system (GE Healthcare, Chicago, IL, USA; cat. no. 34080) according to the manufacturer's instructions. After incubation with a fluorophore-conjugated secondary antibody (Bio-Rad, Hercules, CA, USA; dilution 1:2000)) for 1 h at RT, the protein was directly detected using a ChemiDoc MP Imaging System (BioRad, Hercules, CA, USA).

Quartz Crystals Surface Modification

Lectin (Concavalin A; Sigma-Aldrich, St. Louis, MO, USA; L7647) was immobilized on the transducers to create sensors that functioned properly. The sensors were subjected to ethanol sonication, Hellmanex II cleaning (2% v/v), and rinsing with Milli-Q water (Millipore, Burlington, MA, USA). The samples were then dried and exposed to ultraviolet (UV) radiation for half an hour. They were then treated with 95% v/v 3-aminopropyltriethoxysilane (Sigma-Aldrich, St. Louis, MO, USA). After 30 min of immersion in a 2.5% v/v glutaraldehyde (Sigma-Aldrich, St. Louis, MO, USA) aqueous solution, the sensors were washed with water and buffer solution and incubated for one hour in 2.5 mM lectin solutions. Finally, the lectin-functionalized crystals were incubated for 20 min in 4% v/v glycine solution to block the remaining free aldehyde groups.

Combined Quartz Crystal Microbalance with Dissipation and NanoPlasmonic Sensing Interaction Studies of sEVs

The combined QCM-D and NPS measurements were performed using a Q-Sense E1 module with a sapphire window (Biolin Scientific, Sweden) integrated with an Insplorion Acoulyte module (Insplorion AB, Sweden). The experiments used lectin-functionalized Acoulyte AT-cut quartz crystals featuring randomly distributed silica-coated gold nanodisks (~100 nm in diameter, 20 nm in height) on the surface (Insplorion AB, Sweden). These nanodisks exhibit Localized Surface Plasmon Resonance (LSPR), producing an absorption peak (~700 nm) that shifts ($\Delta\lambda$max) with changes in the local refractive index, enabling real-time monitoring of biomolecular interactions. Frequency and dissipation were analyzed using the QTools software (Biolin Scientific, Sweden), and LSPR signals were analyzed using the Insplorer software (Insplorion AB, Sweden). The interactions between sEVs (derived from primary or metastatic cancer cells) and affinity ligand Concanavalin A (Con A) were studied using QCM-D and NPS at a flow rate of 25 μL/min and 37.0°C. The binding buffer was Phosphate-buffered saline (PBS) (pH 7.4, I = 10 mM, 137 mM NaCl, and 2.7 mM KCl). In all cases, the sEVs and buffer were flowed at 25 μL/min, and a sensor was reserved for baseline measurements to account for drift and background changes induced by buffer exchange. The exchange of the sEVs and buffer to verify the interaction study was made possible by two Teflon tubes attached to the module's inlet and exit. To eliminate extra mass and unbound protein from the quartz crystal, a peristaltic pump was used to pump PBS containing 0.25% Tween 20 (PBST) solution for 15–20 min at a rate of 50 μL/min. Following a two-minute period during which a baseline of frequency and dissipation was observed at a flow rate of 25 μL/min, sEVs (derived from primary or metastatic cancer cells) were supplied to monitor the glycan-lectin interaction for the next 30 min. Finally, unbound protein was removed by pumping the PBST solution for 15 min. All experiments were performed on coded samples, ensuring that the operator was blinded to sample identity during data acquisition and analysis.

Flow Induced Dispersion Analysis (FIDA) of the Binding of Fluorescent Labeled Lectins to sEVs Derived From Melanoma Cells

Flow-induced dispersion analysis (FIDA) was conducted using a microfluidic FIDA-1 instrument equipped with an LED excitation wavelength of 480 nm, using FIDA standard capillaries (inner diameter: 75 µm, LT: 1 m, Leff: 84 cm). For FIDA, fluorescently labeled lectin (FITC-concanavalin A, Sigma-Aldrich, St. Louis, MO, USA; C7642) was prepared in a buffer optimized for lectin-glycan interactions (PBS, pH 7.4). Labeled lectin was diluted to an appropriate concentration (1 µg/mL) and incubated with increasing concentrations (10^8–10^{11} particles/mL) of sEVs in a buffered solution (PBS, pH 7.4) to allow binding. Sample analysis was performed by filling the capillary with 4 µL of sEVs solution, followed by injection of 39 nL of labeled lectin, which was mobilized towards the detector with the sEVs solution at 50 mbar for 24 min at 25°C, pH 7.4.

The obtained Taylorgrams were processed using FIDA Data Analysis Software, version 3.0 (Fida Biosystems Aps, Copenhagen, Denmark) to calculate the apparent hydrodynamic radius (R_h) at each analyte (sEVs) concentration. This standardized software-based fitting minimized operator influence, while parallel processing under identical conditions and independent repetitions reduced variability and bias.

First, the diffusion coefficient (D) was determined from Taylorgram, using the following equation:

$$D = \frac{R_c^2 \cdot t_0}{24 \cdot \sigma_t^2}, \tag{1}$$

where R_c is the capillary radius, t_0 is the average elution time of the solute, and σ_t^2 is the temporal variance of the solute peak.[29] The apparent hydrodynamic radius (R_h) was then calculated using the Stokes–Einstein equation:

$$R_h = \frac{k_B \cdot T}{6 \cdot \pi \cdot \eta \cdot D}, \tag{2}$$

where k_B is Boltzmann's constant, T is the absolute temperature, η is the dynamic viscosity of the solvent, and D is the diffusion coefficient.

An increase in R_h indicated the formation of lectin-sEV complexes, allowing quantitative evaluation of the interaction, including the apparent dissociation constant (K_d).

We used the following binding isotherm model (assuming 1:1 binding) for the obtained values of the apparent hydrodynamic radius (R_h) as a function of the sEVs concentration ($[A]$):

$$R_h = \frac{1 + \frac{1}{K_d}[A]}{\left(\frac{1}{R_I} - \frac{1}{R_{IA}}\right) + \left(1 + \frac{1}{K_d}[A]\right)\frac{1}{R_{IA}}}, \tag{3}$$

where R_I and R_{IA} are the indicator (lectin) and complex hydrodynamic radius, respectively, $[A]$ is the formal analyte (sEVs) concentration, and K_d is the dissociation constant.[30] We fit this model to the data while maintaining a fixed value of the hydrodynamic radius of the lectin (R_I) using nonlinear regression analysis methods and R software (R version 4.1.2).

Lectin-Based Cytometry Analysis of Melanoma Cells and sEVs Released by Them

Surface glycosylation of WM115 and WM266-4 melanoma cells was analyzed by flow cytometry using Con A lectin (FITC-concanavalin A, Sigma-Aldrich, St. Louis, MO, USA; C7642) as described in[11] with minor modifications. Briefly, cells (7×10^4 per sample) and sEVs (isolated from 20 mL of conditioned media per sample; 1×10^9 – 6×10^9 sEVs per sample) were incubated for 45 min on ice with Con A-fluorescein isothiocyanate (FITC) conjugate (1 µg/50 µL PBS). Next, the cells and sEVs were washed in PBS, and fluorescence was assessed using the Aurora CS spectral cell sorter (Cytek, California, USA). Control samples without Con A and with Con A blocked for 1 h with competitive sugar, ie 0.5 M methyl-α-D-mannopiranoside, were also prepared. For each sample, 10^4 sEVs and 10^6 cells were analyzed in an Aurora CS spectral cell sorter with 0.1% FSC. Before the analysis, the Aurora CS was calibrated using routine performance tracking SpectroFlo® QC Beads (3 µm particles with one fluorescence intensity at a concentration of 10^7/

mL, Cytek, California, USA, cat. no. SKU B7-10001), following the guidelines of the instrument provider. Analysis of raw data, including the percentage of positive cells/sEVs and mean fluorescence intensity (RFI), was carried out using FlowJo v.10.10. All experiments were performed with at least three biological replicates for all experimental conditions. To compare the RFI of unstained samples, samples stained with Con A, and samples stained with Con A and simultaneously blocked with methyl-α-d-mannopiranoside in WM115 and WM266-4 cells, two-way ANOVA with post-hoc Tukey's test was used. The same analysis was performed to compare the RFI of the sEVs isolated from WM115 and WM266-4 cells. Comparison of RFI normalized to *unstained* samples for both cell lines as well as for sEVs isolated from both cell lines was performed using *t*-test. Statistical analyses were performed using Prism 10.2.3 (GraphPad Software Inc., La Jolla, CA, USA).

Results and Discussion

Characterization of Small Extracellular Vesicles

The sEVs released by WM115 and WM266-4 melanoma cells were isolated from the conditioned medium by differential ultracentrifugation. Nanoparticle Tracking Analysis (NTA) was used to determine the size and concentration of isolated sEVs. For both cell lines, analyzed sEVs represent homogenous populations with mean diameter of vesicle equal 115.5 nm and 146.5 nm, respectively for WM115- and WM266-4-derived sEVs (Figure 2A). NTA also revealed that metastatic WM266-4 melanoma cells secreted larger vesicles than did primary WM115 melanoma cells (Figure 2B). Interestingly, while Saroj et al reported that breast cancer–derived EVs were smaller than those from epithelial breast cells, our NTA data revealed the opposite trend in melanoma, with metastatic WM266-4 cells secreting larger vesicles than their primary WM115 counterparts. This indicates that EV size is not a universal hallmark of malignancy but instead varies with the type of cell and the stage of disease progression.[24] The statistical significance of the difference between the mean diameters of the sEVs released by WM115 and WM266-4 cells was confirmed by the results of the *t*-test ($p \leq 0.0001$). However, it seems that primary WM115 melanoma cells secreted 1.7 × more vesicles than WM266-4 cells, indicating significant differences in the number of sEVs derived from WM155 and WM266-4 cells, which was confirmed by the results of the Mann–Whitney test ($p \leq 0.05$) (Figure 2C). Western blot analysis of exosome protein markers (CD81, CD63, Flotillin-1 and Tsg101) revealed that the isolated fraction of vesicles was enriched in exosomes (Figure 2D and E).

The purity of isolated sEVs was confirmed by the lack of Golgi (Grp78) and mitochondrial (TOM20) markers in sEV fractions (Figure 2F). Despite the fact that 20 µg of each lysate was used for the Western blotting analysis, the levels of individual exosome markers differ between sEV fractions derived from WM115 and WM266-4 cells. This discrepancy may result from altered glycosylation of sEVs derived from WM266-4 cells, which can mask antibody-binding sites, thereby reducing detection efficiency in immunoassays such as Western blotting.[31] Therefore, to overcome this limitation and gain a more accurate view of surface glycan alterations, we employed biophysical glycoprofiling techniques, including Quartz Crystal Microbalance with Dissipation monitoring combined with NanoPlasmonic Sensing, and Flow-Induced Dispersion Analysis, which allow label-free or solution-based analysis of glycan–lectin interactions and are unaffected by epitope masking.

Combined Quartz Crystal Microbalance with Dissipation and NanoPlasmonic Sensing Interaction Studies of sEVs

Based on previous studies conducted on melanoma cells at different stages of tumor progression,[20,21] we wondered whether it would be possible to distinguish sEVs samples released by primary and metastatic cells by analyzing their glycosylation profiles. To investigate this, we combined QCM-D and NPS, utilizing silica-coated nanostructured gold–quartz sensors functionalized with Con A lectin. Changes in the frequency, dissipation, and LSPR peak position shifts with time (in min) are presented in Figure 3A and B, respectively.

After stabilization in running buffer, sEVs (concentration determined by NTA: $5.0 \times 10^{\square}$ particles/mL) were introduced over the sensor at a flow rate of 25 µL/min until saturation was achieved. The resonance frequency (F) decreased more significantly for WM266-4-derived sEVs (metastatic, black), exhibiting a drop approximately twice as large as that observed for WM115-derived sEVs (primary, grey), suggesting enhanced mass adsorption (Figure 3A).

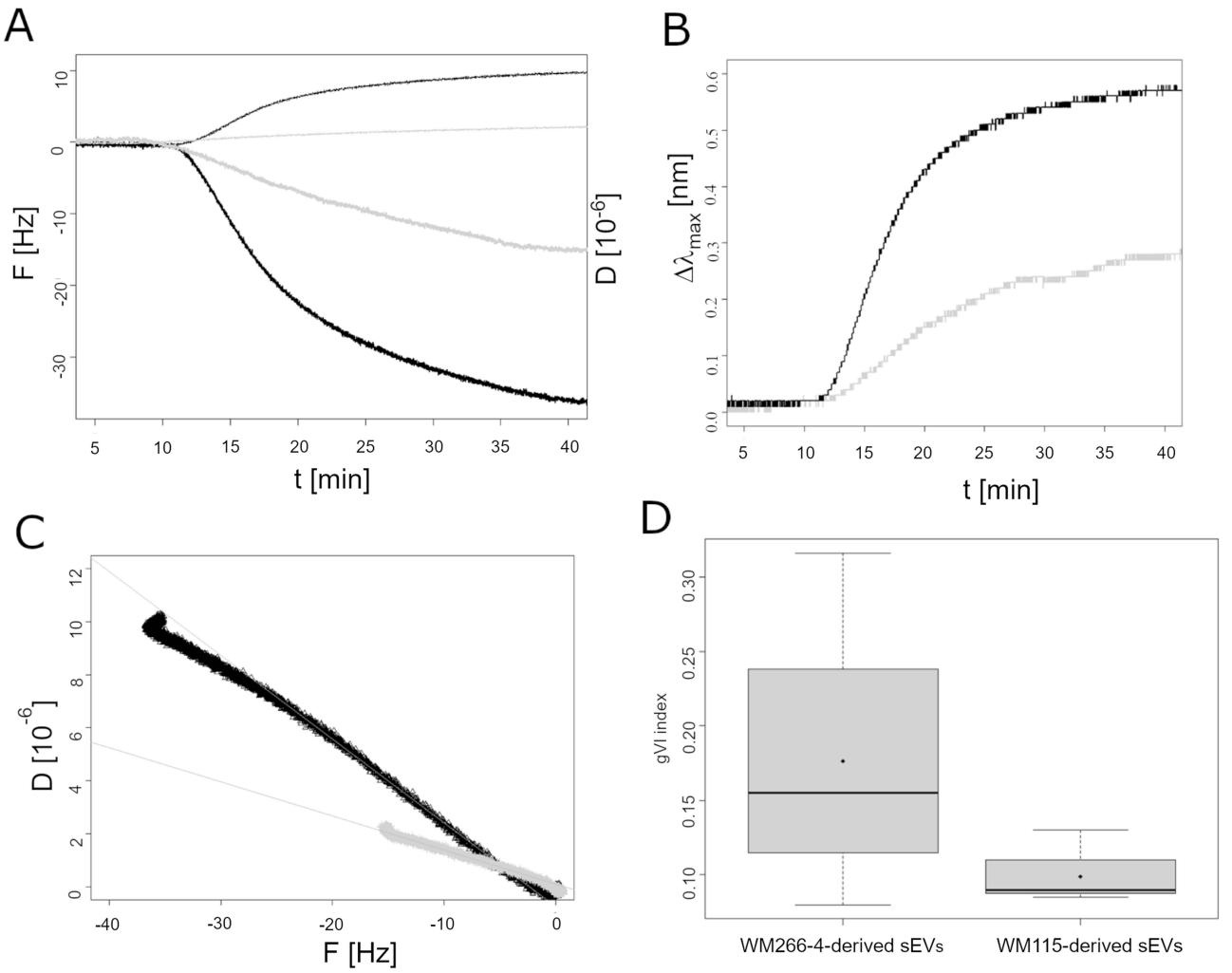

Figure 3 Results of the combined QCM-D/NPS lectin–glycan interaction study using sEVs released by primary melanoma (WM115, grey) and lymph node metastatic (WM266-4,black) cell lines. (**A**) QCM-D sensograms showing the time courses of frequency (*F*) and dissipation (*D*) changes upon sEVs binding. (**B**) NPS sensograms illustrating LSPR peak position ($\Delta\lambda_{max}$) shifts with time during lectin–sEV interactions. (**C**) Representative plots of dissipation (*D*) against frequency (*F*) changes for the 7th overtone from QCM-D measurements of Con A binding to WM115- and WM266-4-derived sEVs. (**D**) Boxplots summarizing gVI index values obtained for Con A interactions with each sEV type.

Concurrently, dissipation (*D*) showed a slight increase for WM115-derived sEVs and a pronounced increase for WM266-4-derived sEVs, consistent with the efficient capture of sEVs onto the sensor surface and indicating differences in viscoelastic properties (Figure 3A). Simultaneously, a progressive shift of the LSPR band was observed, with the shift for WM266-4-derived sEVs (metastatic, black) being approximately twice as large as that for WM115-derived sEVs (primary, grey), reflecting altered surface interactions (Figure 3B). Notably, both QCM-D and NPS signals approached saturation within a comparable timeframe, reflecting consistent kinetic profiles across techniques. To quantify these changes, we calculated the glycan viscoelasticity index (gVI), which correlates with metastatic potential. The gVI index is defined as the absolute value of the slope of the regression line describing the relation between dissipation (*D*) and frequency (*F*) changes.[32] The estimated values of gVI's for primary melanoma (WM115) and lymph node metastatic (WM266-4) cell lines were obtained by fitting the linear regression model to the data recorded during first minutes after lectin introduction (the reference plot for one of analyzed data sets is presented in Figure 3C). The experiment was performed in at least 4 replicates, among sEVs derived from WM115 and WM266-4 cells. The obtained values of gVI index for each group are presented in form of box plots in Figure 3D. The results show substantial variability in the viscoelastic index values for sEVs derived from WM266-4 cells. The average viscoelastic index for this group (mean = 0.1765, median = 0.155, SD = 0.099) was approximately twice as high as that observed for WM115-derived sEVs (mean

= 0.09875, median = 0.09, SD = 0.02), indicating significant differences in the viscoelastic properties of vesicles from metastatic versus primary melanoma cells. Statistical significance of difference between gVI index values for both cell lines was confirmed by results of the Welch test ($p<0.01$) and analysis of covariance (ANCOVA) method ($p<0.01$) used for comparison of fitted regression slopes.[33]

Flow Induced Dispersion Analysis of the Binding of Fluorescent Labeled Lectins to sEVs Derived From Melanoma Cells

Owing to the high sample requirements of the quartz crystal microbalance with dissipation monitoring, Flow-Induced Dispersion Analysis was employed as an alternative technique to quantify the binding affinity of fluorescently labeled lectins to sEVs derived from melanoma cell lines. FIDA is a solution-phase, immobilization-free method that enables accurate determination of dissociation constants (K_d) under near-physiological conditions. By monitoring changes in the apparent hydrodynamic radius (R_h) of a fluorescent indicator upon interaction with a non-labeled analyte, FIDA offers a sensitive approach for characterizing molecular interactions. Although FIDA has not been applied to lectin–sEV systems, previous studies have demonstrated its utility in analyzing a wide range of biomolecular interactions, including antibody–antigen binding, aptamer–target complexes, and surface markers on extracellular vesicles.[29,34] The technique's low sample consumption and compatibility with native conditions make it particularly well-suited for studies involving limited or precious materials, such as patient-derived sEVs.

In this study, Con A labeled with FITC was used as a fluorescent indicator and maintained at a constant concentration. The sEVs released by WM266-4 (metastatic melanoma) and WM115 (primary melanoma) cells were titrated into the system over a concentration range of 10^8–10^{11} particles/mL. As the concentration of sEVs increased, the diffusion behavior of Con A-FITC changed, indicating the formation of complexes with vesicles. Time-resolved fluorescence detection generated Taylorgrams, which were analyzed to extract the diffusion coefficient (D) (Equation 1) and calculate the apparent hydrodynamic radius (R_h) using the Stokes–Einstein equation (Equation 2). The binding isotherm model (Equation 3) was fitted to the obtained values of the apparent hydrodynamic radius (R_h) measurements for different sEVs concentrations by nonlinear regression analysis methods. We used these models with a fixed value for the hydrodynamic radius of lectin (R_l) to obtain the corresponding binding isotherm curves for WM266-4-derived sEVs and WM115-derived sEVs. Figure 4 shows a plot of the binding curves obtained for a representative dataset.

Having the binding isotherm models fitted for WM266-4-derived sEVs and WM115-derived sEVs, we obtained the values of apparent dissociation constants (K_d) (Equation 3). The analysis revealed stronger binding of Con A to WM266-4-derived sEVs (K_d = 3.06×10^9 particles/mL) compared to WM115-derived sEVs (K_d = 9.16×10^9 particles/mL), indicating a higher affinity of the lectin for sEVs from the metastatic cell line. Statistical significance of difference

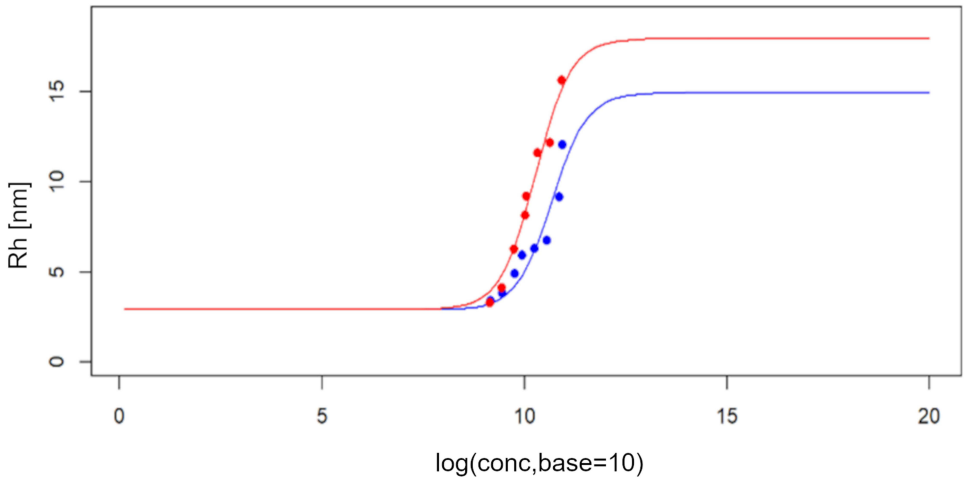

Figure 4 Observed values of apparent hydrodynamic radius (R_h) of Con A-FITC as a function of sEVs concentration with fitted binding isotherm curves for WM266-4-derived sEVs (red) and WM115-derived sEVs (blue), respectively. The plot is represented on a logarithmic scale for the x-axis (sEVs concentration).

https://doi.org/10.2147/NSA.S547649

between K_d values for both cell lines was confirmed by results of the Wald test comparing parameters of two fitted binding isotherm models ($p<0.01$) and analysis of variance (ANOVA) using pooled model method ($p<0.01$).

These results are consistent with previous observations in cell-based assays, where Con A exhibited a greater binding affinity to metastatic melanoma cells than to cells derived from primary tumors.[20,21] Notably, the binding curve for WM266-4-derived sEVs displayed a steeper transition region, suggesting multivalent interactions, likely due to the presence of multiple high-affinity glycan motifs on the surface of metastatic cell-derived sEVs. This behavior is characteristic of lectins engaging multiple glycosylation sites simultaneously and is in agreement with prior studies highlighting the multivalent nature of lectin-glycoconjugate interactions.[35,36] In conclusion, this study demonstrates the utility of FIDA for quantifying lectin-sEV interactions and determining K_d values in solution without the need for immobilization or secondary labeling.

Recent advances incorporating the C-jump method into FIDA workflows have significantly broadened the applicability of this technique to complex biological environments, including direct measurements in human serum. C-jump enables kinetic analysis by inducing rapid concentration changes within a microfluidic system, preserving native conditions while allowing the precise extraction of both association and dissociation rates. Its demonstrated compatibility with 90% human serum and its ability to operate in a label-free manner, as shown for protein–protein and protein–small molecule interactions,[37] strongly supports its potential extension to lectin–sEV systems. This development opens a compelling avenue for future studies of glycan-mediated vesicle interactions under physiologically relevant conditions.

The observed differences in binding affinities between sEVs from metastatic and primary melanoma cells emphasize the role of surface glycosylation in sEV biology and underscore the potential of FIDA in glyco-interactomics and extracellular vesicle characterization. Importantly, these findings are in agreement with our combined QCM-D/NPS study, further validating the observed differences in lectin-binding affinities between the sEV subtypes derived from melanoma cells.

Cytometry Analysis of Surface Glycosylation of Primary and Metastatic Melanoma Cells and Melanoma-Derived sEVs

We have previously demonstrated, by means AFM/QCM-D, that Con A has a higher affinity for surface glycans in metastatic melanoma cells compared to primary melanoma cells.[20,21] Additionally, QCM-D/NPS and FIDA analyses of the dissociation of lectin-glycan complexes revealed that the affinity of ConA for the surface glycans of metastatic melanoma-derived sEVs was higher than that of primary melanoma-derived sEVs (Figures 3 and 4).

Flow cytometry was performed to verify the enrichment of ConA-specific glycoepitopes in the metastatic melanoma cells. By applying lectin ConA conjugated with FITC, the surface glycosylation of metastatic and primary melanoma cells and sEVs derived from these cells was performed (Figure 5).

The specificity of Con A binding to the surface of melanoma cells or melanoma-derived sEVs was verified by simultaneous Con A staining and blocking with methyl-α-D-mannopiranoside (*blocked* samples, Figure 5A and B). Both *blocked* and *unstained* samples exert similar fluorescence intensity (RFI) in cell analysis as well as in sEVs analysis. This confirmed that observed increase of fluorescence for Con A samples is a result of specific Con A binding. Statistical significance of difference between RFI of *unstained/ blocked* sample and *ConA* (stained with Con A) sample of WM115 and WM266-4 cells as well as between RFI of *unstained /blocked* sample and *ConA* sample of WM115-derived sEVs and WM266-4-derived sEVs was confirmed by results of the two-way ANOVA with post-hoc Tukey's test (see Figure 5A and B for details). Moreover, this statistic analysis confirmed also significance of difference between *ConA* sample of WM115 cells and *ConA* sample of WM266-4 cells as well as between *ConA* sample of WM115-derived sEVs and *ConA* sample of WM266-4-derived sEVs ($p \leq 0.05$). It was found that primary melanoma (WM115) and metastatic melanoma (WM266-4) cells interact with Con A (Figure 5C), however the shift of ConA fluorescence (*unstained* vs *ConA*) was higher for WM266-4 cells (Figure 5E). Nonetheless, statistical analysis of normalized RFI for WM115 cells and WM266-4 cells by using *t*-test was not confirmed significant differences. Additionally, analysis of Con A interaction with melanoma-derived sEVs revealed similar results (Figure 5D). The difference in Con A binding (metastatic vs primary) was more pronounced in sEVs than in cells. Namely, analysis showed significantly higher affinity of ConA to WM266-4-derived sEVs than to

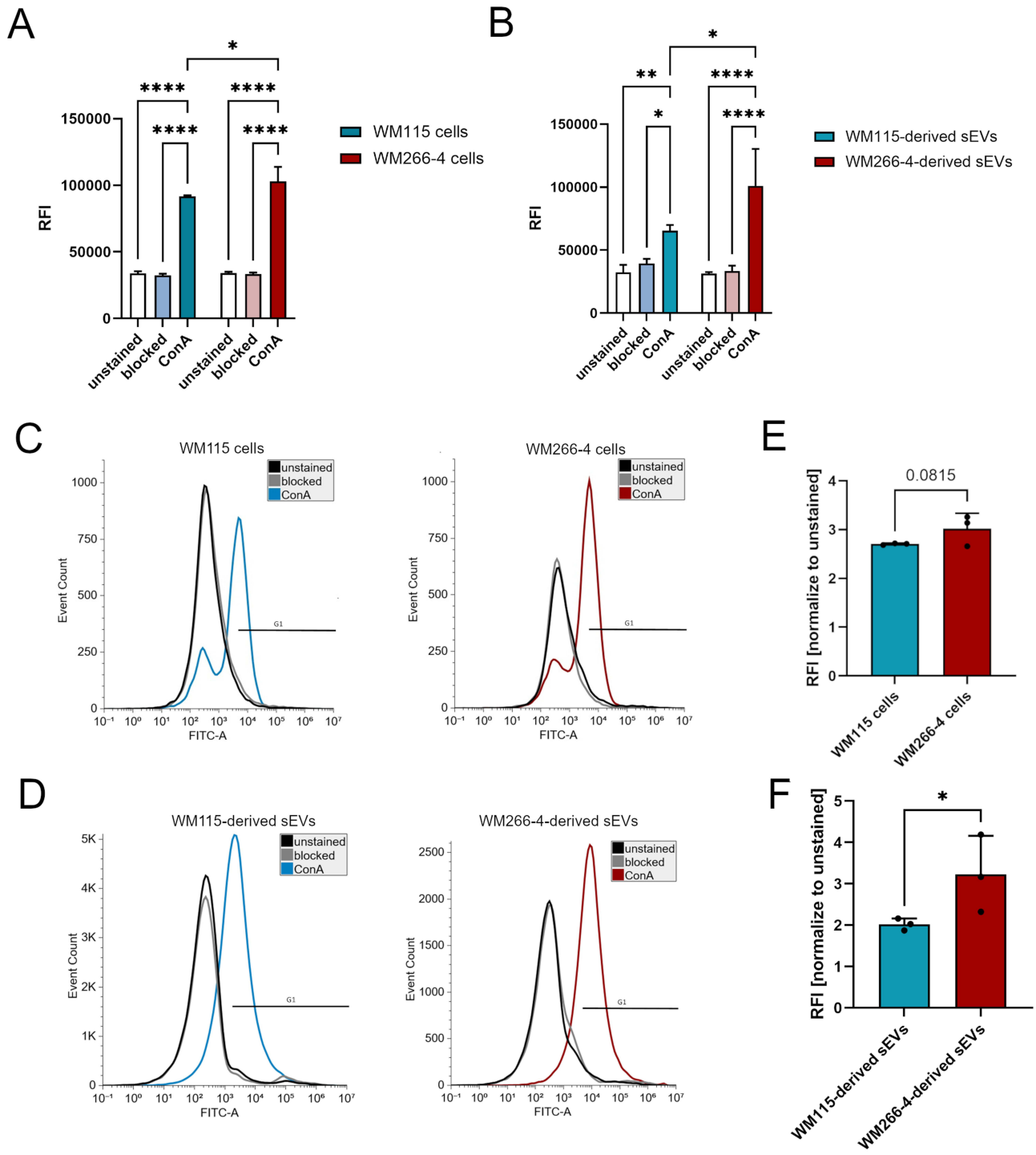

Figure 5 Flow cytometry analysis of surface glycosylation of WM115 and WM266-4 melanoma cells and melanoma-derived sEVs. (**A** and **B**) Analysis of the relative fluorescence intensity (RFI) for WM115 and WM266-4 melanoma cells (**A**) and WM115- and WM266-4-derived sEVs (**B**) stained with ConA (*ConA*), stained with ConA and simultaneously blocked with methyl-α-D-mannopiranoside (*blocked*) and unstained ones (*unstained*). Bars: mean value, error bars: SD, n = 3. Statistical significance of difference between RFI of *unstained, blocked* and *ConA* samples for both cell lines and for sEVs isolated from both cell lines as well as between RFI of *ConA* sample for WM115 cells/WM115-derived sEVs and *ConA* sample for WM266-4 cells/WM266-4-derived sEVs was confirmed by results of the two-way ANOVA with post-hoc Tukey's test (* $p \leq 0.05$; ** $p \leq 0.01$; **** $p \leq 0.0001$). (**C** and **D**) Histograms for ConA-positive cells (**C**) and ConA-positive melanoma-derived small extracellular vesicles (sEVs) (**D**). Colored (blue or red) histograms represent staining with ConA lectin, grey histograms represent staining with ConA lectin with simultaneous blocking with methyl-α-D-mannopiranoside and black histograms represents background fluorescence. The X axis shows log fluorescence intensity, Y axis shows the number of events. G1 - gate for ConA positive subjects. (**E and F**) Analysis of the relative fluorescence intensity (RFI) for WM115 and WM266-4 melanoma cells stained with ConA normalized to unstained ones (**E**) and WM115- and WM266-4-derived sEVs stained with ConA normalized to unstained ones (**F**). Bars: mean value, error bars: SD, n = 3. Statistical significance of difference between normalized RFI for both cell lines as well as for sEVs isolated from both cell lines was confirmed by results of the *t*-test (* $p \leq 0.05$).

https://doi.org/10.2147/NSA.S547649

WM115-derived sEVs (Figure 5F). Statistical significance of difference between RFI normalized to *unstained* sample of WM115-derived sEVs and WM266-4-derived sEVs was confirmed by results of the *t*-test ($p \leq 0.05$). Cytometry analysis confirmed differences in lectin affinity between primary and metastatic melanoma cells as well as between sEVs derived from primary or metastatic melanoma cells. This observation is consistent with earlier studies demonstrating that EVs preserve glycosylation patterns reflective of their parental cells, thereby providing a glycomic "fingerprint" of disease state.[38,39] In comparison with FIDA or QCM-D/NPS analyses, cytometric measurements is less sensitive, nevertheless, still is able to identify differences in lectin binding in analysed model. Additionally, cytometry analysis is more accessible, when thinking about diagnostic potential of surface glycosylation pattern in melanoma cell and sEVs.

Conclusion

This study presents a comprehensive multimodal biophysical and biochemical characterization of small extracellular vesicles derived from primary and metastatic melanoma cells, underscoring their potential as functional nanobiomaterials with surface signatures associated with malignancy. Nanoparticle Tracking Analysis revealed that metastatic WM266-4 cells secreted fewer but larger sEVs than their primary WM115 counterparts. Western blotting confirmed exosomal identity and high purity of the vesicle preparations; however, variability in exosomal marker detection suggests that altered glycosylation may occlude antibody-binding epitopes, thereby affecting immunodetection sensitivity.

To probe vesicle surface architecture in greater depth, we applied a suite of complementary biophysical glycoprofiling techniques, including Quartz Crystal Microbalance with Dissipation monitoring, Nanoplasmonic Sensing, and, for the first time in this context, Flow-Induced Dispersion Analysis. These techniques were used to quantify the lectin-EV interactions under near-native conditions. Our findings revealed significantly elevated Concanavalin A binding and enhanced viscoelastic glycan properties in metastatic sEVs, consistent with a denser and more accessible glycan coating. Although less sensitive, flow cytometry supported these trends and further demonstrated its compatibility with translational diagnostics.

Together, these data confirm that surface glycosylation patterns serve as robust functional biomarkers capable of distinguishing sEV subtypes according to their metastatic origin. Specifically, we demonstrated that the glycan profile of melanoma-derived sEVs is reflective of the malignant state, yielding a quantifiable and biologically relevant signature.

Although conventional protein-based markers have provided essential insights into vesicle biology, they often lack the sensitivity and specificity required to resolve the functional heterogeneity associated with malignant transformation. Glycosylation represents a dynamic post-translational layer of biological regulation that responds to oncogenic signaling, metabolic reprogramming, and therapeutic intervention. Thus, the structurally diverse and environmentally responsive glycan coat offers a richer and more adaptable biomolecular interface than the protein epitopes alone. Glycoprofiling, therefore, not only enables enhanced diagnostic resolution but also offers a pathway to monitor therapy responsiveness and identify novel therapeutic targets centered on aberrant glycosylation.

Notably, recent advances in FIDA using the C-jump approach have substantially broadened the potential of this platform for clinical translation. By enabling the direct measurement of kinetic binding parameters in highly complex matrices such as human serum, C-jump-enhanced FIDA eliminates the need for immobilization, minimizes sample requirements, and permits label-free detection. These capabilities were recently demonstrated in the quantification of protein–protein and protein–small molecule interactions under physiological conditions. Extending this approach to lectin–sEV systems could facilitate the real-time in-solution glycoprofiling of patient-derived vesicles, greatly enhancing the clinical relevance and translational utility of this methodology in liquid biopsy applications.

In conclusion, by placing the vesicle glycome at the forefront of nanobiomarker discovery, this study provides a foundation for next-generation glyco-nanodiagnostics and personalized therapeutic strategies for melanoma and other glycosylation-driven diseases. Our findings suggest that sEV glycoprofiling is a powerful, mechanistically informative, and biophysically tractable modality for precision oncology; however, we acknowledge that the present results are correlative and require further validation in clinically derived samples. Expanding the analysis to a broader panel of lectins and incorporating complementary glycomic approaches will be crucial to refine and extend these observations.

Acknowledgments

This work was supported by the Warsaw University of Technology under the NCHEM4 grant. The acquisition of experimental equipment (Insplorion Acoulyte module) was partially funded by the Warsaw University of Technology within the IDUB program (apparatus grant) and by the Alexander von Humboldt Foundation through the Research Group Linkage program. The authors also acknowledge BioTech a.s. and Fida Biosystems ApS for their support in enabling the experiments using the FIDA-1 instrument. The lectin-based cytometry analysis was performed using the Aurora CS spectral cell sorter, the purchase of which has been supported by a grant from the Priority Research Area (POB BioS) under the Strategic Programme Excellence Initiative at Jagiellonian University.

Disclosure

The authors report no conflicts of interest in this work.

References

1. Bray F, Laversanne M, Sung H, et al. Global cancer statistics 2022: GLOBOCAN estimates of incidence and mortality worldwide for 36 cancers in 185 countries. *CA Cancer J Clin*. 2024;74(3):229–263. doi:10.3322/caac.21834
2. Berk-Krauss J, Stein JA, Weber J, Polsky D, Geller AC. New systematic therapies and trends in cutaneous melanoma deaths among US whites, 1986-2016. *Am J Public Health*. 2020;110(5):731–733. doi:10.2105/AJPH.2020.305567
3. Helgadottir H, Mikiver R, Schultz K, et al. Melanoma incidence and mortality trends among patients aged 59 years or younger in Sweden. *JAMA Dermatol*. 2024;160(11):1201–1210. doi:10.1001/jamadermatol.2024.3514
4. Thomas S, Hoyt D, Stoddard G, et al. Declining invasive and rising in situ melanoma incidence trends in Iceland: a nationwide cohort study. *J Eur Acad Dermatol Venereol JEADV*. 2025;39(7):1278–1284. doi:10.1111/jdv.20386
5. Zhou L, Zhong Y, Han L, Xie Y, Wan M. Global, regional, and national trends in the burden of melanoma and non-melanoma skin cancer: insights from the global burden of disease study 1990–2021. *Sci Rep*. 2025;15(1):5996. doi:10.1038/s41598-025-90485-3
6. Lo SN, Williams GJ, Cust AE, et al. Long-term survival across Breslow thickness categories: findings from a population-based study of 210 042 Australian melanoma patients. *JNCI J Natl Cancer Inst*. 2025;117(1):152–156. doi:10.1093/jnci/djae198
7. Sobiepanek A, Paone A, Cutruzzolà F, Kobiela T. Biophysical characterization of melanoma cell phenotype markers during metastatic progression. *Eur Biophys J*. 2021;50(3–4):523–542. doi:10.1007/s00249-021-01514-8
8. Hoja-Łukowicz D, Przybyło M, Duda M, Pocheć E, Bubka M. On the trail of the glycan codes stored in cancer-related cell adhesion proteins. *Biochim Biophys Acta Gen Subj*. 2017;1861(1):3237–3257. doi:10.1016/j.bbagen.2016.08.007
9. Stępień EŁ, Kamińska A, Surman M, Karbowska D, Wróbel A, Przybyło M. Fourier-transform InfraRed (FT-IR) spectroscopy to show alterations in molecular composition of EV subpopulations from melanoma cell lines in different malignancy. *Biochem Biophys Rep*. 2021;25:100888. doi:10.1016/j.bbrep.2020.100888
10. Surman M, Przybyło M, Wilczak M. Melanoma-derived extracellular vesicles transfer proangiogenic factors. *Oncol Res*. 2025;33(2):245–262. doi:10.32604/or.2024.055449
11. Surman M, Hoja-Łukowicz D, Szwed S, Drożdż A, Stępień E, Przybyło M. Human melanoma-derived ectosomes are enriched with specific glycan epitopes. *Life Sci*. 2018;207:395–411. doi:10.1016/j.lfs.2018.06.026
12. Wilczak M, Surman M, Przybyło M. The role of intracellular and extracellular vesicles in the development of therapy resistance in cancer. *Curr Pharm Des*. 2024;30(35):2765–2784. doi:10.2174/0113816128326325240723051625
13. Zhou Q, Wang J, Zhang Z, Wuethrich A, Lobb RJ, Trau M. Tracking the EMT-like phenotype switching during targeted therapy in melanoma by analyzing extracellular vesicle phenotypes. *Biosens Bioelectron*. 2024;244:115819. doi:10.1016/j.bios.2023.115819
14. Gauthier SA, Pérez-González R, Sharma A, et al. Enhanced exosome secretion in down syndrome brain - a protective mechanism to alleviate neuronal endosomal abnormalities. *Acta Neuropathol Commun*. 2017;5(1):65. doi:10.1186/s40478-017-0466-0
15. Lobb RJ, Lima LG, Möller A. Exosomes: key mediators of metastasis and pre-metastatic niche formation. *Semin Cell Dev Biol*. 2017;67:3–10. doi:10.1016/j.semcdb.2017.01.004
16. Surman M, Jankowska U, Wilczak M, Przybyło M. Similarities and differences in the protein composition of cutaneous melanoma cells and their exosomes identified by mass spectrometry. *Cancers*. 2023;15(4):1097. doi:10.3390/cancers15041097
17. Surman M, Stępień E, Przybyło M. Melanoma-derived extracellular vesicles: focus on their proteome. *Proteomes*. 2019;7(2):21. doi:10.3390/proteomes7020021
18. Syn N, Wang L, Sethi G, Thiery JP, Goh BC. Exosome-mediated metastasis: from epithelial–mesenchymal transition to escape from immunosurveillance. *Trends Pharmacol Sci*. 2016;37(7):606–617. doi:10.1016/j.tips.2016.04.006
19. Li P, Xu X, Zhang C, et al. Glycosylation on extracellular vesicles and its detection strategy: paving the way for clinical use. *Int J Biol Macromol*. 2025;295:139714. doi:10.1016/j.ijbiomac.2025.139714
20. Sobiepanek A, Kowalska PD, Szota M, et al. Novel diagnostic and prognostic factors for the advanced melanoma based on the glycosylation-related changes studied by biophysical profiling methods. *Biosens Bioelectron*. 2022;203:114046. doi:10.1016/j.bios.2022.114046
21. Sobiepanek A, Milner-Krawczyk M, Lekka M, Kobiela T. AFM and QCM-D as tools for the distinction of melanoma cells with a different metastatic potential. *Biosens Bioelectron*. 2017;93:274–281. doi:10.1016/j.bios.2016.08.088
22. Williams C, Royo F, Aizpurua-Olaizola O, et al. Glycosylation of extracellular vesicles: current knowledge, tools and clinical perspectives. *J Extracell Vesicles*. 2018;7(1):1442985. doi:10.1080/20013078.2018.1442985
23. Vrablova V, Kosutova N, Blsakova A, et al. Glycosylation in extracellular vesicles: isolation, characterization, composition, analysis and clinical applications. *Biotechnol Adv*. 2023;67:108196. doi:10.1016/j.biotechadv.2023.108196

24. Saroj S, Paul D, Ali A, Andreou C, Pal S, Rakshit T. Probing aberrantly glycosylated mucin 1 in breast cancer extracellular vesicles. *ACS Appl Bio Mater*. 2023;6(11):4944–4951. doi:10.1021/acsabm.3c00651
25. Zhang G, Huang X, Gong Y, et al. Fingerprint profiling of glycans on extracellular vesicles via lectin-induced aggregation strategy for precise cancer diagnostics. *J Am Chem Soc*. 2024;146(42):29053–29063. doi:10.1021/jacs.4c10390
26. Sun X, Chen B, Shan Y, Jian M, Wang Z. Lectin microarray based glycan profiling of exosomes for dynamic monitoring of colorectal cancer progression. *Anal Chim Acta*. 2024;1316:342819. doi:10.1016/j.aca.2024.342819
27. Mazouzi Y, Sallem F, Farina F, et al. Biosensing extracellular vesicle subpopulations in neurodegenerative disease conditions. *ACS Sens*. 2022;7(6):1657–1665. doi:10.1021/acssensors.1c02658
28. Głuchowska A, Cysewski D, Baj-Krzyworzeka M, et al. Unbiased proteomic analysis of extracellular vesicles secreted by senescent human vascular smooth muscle cells reveals their ability to modulate immune cell functions. *GeroScience*. 2022;44(6):2863–2884. doi:10.1007/s11357-022-00625-0
29. Poulsen NN, Andersen NZ, Østergaard J, Zhuang G, Petersen NJ, Jensen H. Flow induced dispersion analysis rapidly quantifies proteins in human plasma samples. *Analyst*. 2015;140(13):4365–4369. doi:10.1039/C5AN00697J
30. Pedersen ME, Gad SI, Østergaard J, Jensen H. Protein characterization in 3D: size, folding, and functional assessment in a unified approach. *Anal Chem*. 2019;91(8):4975–4979. doi:10.1021/acs.analchem.9b00537
31. Liang Y, Eng WS, Colquhoun DR, Dinglasan RR, Graham DR, Mahal LK. Complex N-linked glycans serve as a determinant for exosome/microvesicle cargo recruitment. *J Biol Chem*. 2014;289(47):32526–32537. doi:10.1074/jbc.M114.606269
32. Kobiela T, Wojciechowski K, Jachimska B. Probing bio interfaces with biophysical methods: aspects of applying the QCM-D method. *Encyclopedia Solid-Liquid Interfaces Elsevier*. 2024:714–722. doi:10.1016/B978-0-323-85669-0.00076-3
33. Andrade JM, Estévez-Pérez MG. Statistical comparison of the slopes of two regression lines: a tutorial. *Anal Chim Acta*. 2014;838:1–12. doi:10.1016/j.aca.2014.04.057
34. Pedersen ME, Østergaard J, Jensen H. Flow-induced dispersion analysis (FIDA) for protein quantification and characterization. In: Phillips TM, editor. *Clinical Applications of Capillary Electrophoresis. Vol 1972. Methods in Molecular Biology*. New York: Springer; 2019:109–123. doi:10.1007/978-1-4939-9213-3_8
35. Dam TK, Hohman O, Sheppard L, Brewer CF, Bandyopadhyay P. Mechanism of multivalent glycoconjugate–lectin interaction: an update. *Adv Carbohydr Chem Biochem*. 2023;84:1–21. doi:10.1016/bs.accb.2023.10.004
36. Martínez-Bailén M, Rojo J, Ramos-Soriano J. Multivalent glycosystems for human lectins. *Chem Soc Rev*. 2023;52(2):536–572. doi:10.1039/D2CS00736C
37. Willmer P, Stender EGP, Sahni Ray K, Hundahl AC, Marie R, Jensen H. In-solution characterization of biomolecular interaction kinetics under native conditions. *Anal Chem*. 2025;97(36):19498–19504. doi:10.1021/acs.analchem.5c02164
38. Zhang J, Qin Y, Jiang Q, et al. Glycopattern alteration of glycoproteins in gastrointestinal cancer cell lines and their cell-derived exosomes. *J Proteome Res*. 2022;21(8):1876–1893. doi:10.1021/acs.jproteome.2c00159
39. Batista BS, Eng WS, Pilobello KT, Hendricks-Muñoz KD, Mahal LK. Identification of a conserved glycan signature for microvesicles. *J Proteome Res*. 2011;10(10):4624–4633. doi:10.1021/pr200434y